RSC Advances

PAPER

View Article Online
View Journal | View Issue

Cite this: *RSC Adv.*, 2025, **15**, 9657

Molecular recognition and potentiometric determination of neostigmine and pyridostigmine by a methylene-bridged naphthotube†

Jian-Fang Wu,‡[ab] Wen-Jie Chen,‡[b] Li-Li Wang,[b] Liu-Pan Yang,*[b] Yan-Fang Wang*[cd] and Dehua Liao*[a]

Received 26th December 2024
Accepted 24th March 2025

DOI: 10.1039/d4ra09021g

rsc.li/rsc-advances

A macrocyclic arene featuring rigid bis-naphthalene possesses a remarkable ability to strongly bind neostigmine ($K_a = 2.7 \times 10^4$ M^{-1}) and pyridostigmine ($K_a = 2.2 \times 10^5$ M^{-1}) within its deep cavity. This facilitates the host as a potential ionophore for the potentiometric determination of neostigmine and pyridostigmine with low detection limits of 1.0 μM, highlighting its promising applications in pharmaceutical analysis.

Anticholinesterase agents, also known as indirect-acting cholinomimetics, are a class of drugs that can bind to acetylcholinesterase and inhibit its activity, leading to the accumulation of acetylcholine at nerve terminals and exerting an excitatory effect on cholinergic receptors.[1] Neostigmine (**NEO**) and pyridostigmine (**PYR**) are two of the most representative reversible acetylcholinesterase inhibitors, which form complexes with the anionic site of acetylcholinesterase through their positively charged quaternary ammonium groups to inhibit the enzyme's activity. These two drugs are the most widely used acetylcholinesterase inhibitors in clinical practice, mainly for the treatment of myasthenia gravis, postoperative abdominal distension, urinary retention, paralytic ileus, glaucoma, and reversal of neuromuscular blockade.[2] The development of simple analytical methods for **NEO** and **PYR** is of great significance for drug quality control and the study of drug metabolism kinetics. Several methods have been reported for the determination of drugs in different dosage forms and biological fluids, including high-performance liquid chromatography (**HPLC**),[3] gas chromatography,[4] spectrophotometry,[5] potentiometric titration,[6] *etc.* Among these methods, **HPLC** is the most widely studied due to its high accuracy, however, this method requires complex sample preparation and is time-consuming.[7] Therefore, developing more efficient and rapid methods for the detection of **NEO** and **PYR** is of significant importance.

Since the last century, ion-selective electrodes (**ISEs**) have been widely used in drug analysis and clinical testing due to their simple operation, efficiency, and ease of on-site monitoring.[8] The principle of **ISEs** relies on the partition equilibrium of analytes at the liquid–membrane interface, where the binding affinity of ionophores toward target analytes fundamentally governs both the sensitivity and selectivity of the electrode. Classical macrocyclic hosts such as cyclodextrins and calixarenes have been successfully employed for detecting quaternary ammonium pharmaceuticals. For instance, El-Rahman's research group fabricated an ion-selective electrode utilizing calixarene-based ion carriers, achieving potentiometric detection of **NEO** with excellent selectivity and a linear response range.[9a] Similarly, Khorshid's team developed a β-cyclodextrin-modified carbon paste sensor that demonstrated enhanced performance with a lower detection limit of 6.3×10^{-8} mol L^{-1} for **NEO**.[9b] However, these conventional macrocyclic hosts suffer from certain limitations when employed as ion carriers. Cyclodextrins and sulfonated calixarenes exhibit high water solubility, leading to ionophore leaching and subsequent signal drift during operation.[10] Additionally, the inherent conformational flexibility of calixarenes compromises their binding specificity. Consequently, to achieve superior detection performance, the development of novel macrocyclic hosts featuring rigid architectures and enhanced hydrophobicity is imperative for advanced ion carrier applications.

In recent years, macrocyclic arenes with methylene bridges have attracted wide attention due to their simple synthesis, diverse structures, and ease of modification.[11] The majority of macrocyclic arenes are formed by planar aromatic rings connected by methylene bridges, where the free rotation of the two single bonds around the methylene group can lead to collapse

[a]*Department of Pharmacy, Hunan Cancer Hospital, The Affiliated Cancer Hospital of Xiangya School of Medicine, Central South University, Changsha, Hunan 410000, China. E-mail: liaodehua1125@126.com*

[b]*School of Pharmaceutical Science, Hengyang Medical School, University of South China, Hengyang, Hunan 421001, China. E-mail: yanglp@usc.edu.cn*

[c]*Department of Chemistry, Zhejiang University, Hangzhou 310058, P. R. China. E-mail: 11930562@mail.sustech.edu.cn*

[d]*ZJU-Hangzhou Global Scientific and Technological Innovation Center, ZhejiangUniversity, Hangzhou 311215, P. R. China*

† Electronic supplementary information (ESI) available. See DOI: https://doi.org/10.1039/d4ra09021g

‡ These authors contributed equally to this work.

of the macrocyclic cavity and structural flexibility, limiting their molecular recognition and application performance.[12] To construct macrocyclic arenes with rigid cavities, we synthesized a new type of macrocycle – methylene-bridged naphthotubes using rigidly bridged bisnaphthalenes with an arched structure as building blocks (Fig. 1a).[13] The introduction of the rigid bisnaphthalene[14] structure reduces the involvement of methylene groups during cyclization, decreasing the structural flexibility of the macrocycle while providing a deeper electron-rich cavity (Fig. 1b). Therefore, methylene-bridged naphthotubes exhibit strong binding affinity towards organic cations. Both **NEO** and **PYR** have a positive charge in their structures, leading us to speculate that they are suitable guests for methylene naphthotubes. Herein, in this study, we have re-synthesized the macrocyclic host (**H1**) to ensure its structural integrity and purity for subsequent investigations. We report the binding behavior of **H1** toward **NEO** and **PYR**, and further utilize the host as an ionophore to construct ion-selective electrodes, enabling accurate detection of these two drugs in different formulations and fetal bovine serum.

Initially, we investigated the binding interactions between host **H1** and guests **NEO** and **PYR** in solution (Fig. 2). The ^{1}H NMR spectrum of an equimolar mixture of host **H1** and **NEO** in CD_2Cl_2 revealed a singular set of resonances, indicating the formation of a new complex (**NEO@H1**). This observation suggests that the binding process occurs *via* fast exchange dynamics. Notably, the signals corresponding to the guest within the complex exhibited broadening and, in some cases, disappeared into the baseline. Additionally, a significant downfield shift ($\Delta\delta = 0.28$ ppm) was observed for the H^3 proton signal of host **H1**. A similar influence was noted with the aromatic cation **PYR**, which also induced notable chemical shifts in the aromatic protons of host **H1**. Importantly, the chemical shifts observed for **H1** in the **PYR@H1** complex were generally greater than those seen in **NEO@H1**, suggesting that the binding affinity between host **H1** and **PYR** is stronger than that with **NEO**. Diffusion-ordered spectroscopy (DOSY) experiments (Fig. S1–S3†) reveal a single assembly with diffusion coefficients of 5.97×10^{-10}, 5.56×10^{-10}, and 7.13×10^{-10} $m^2\ s^{-1}$ for **H1**, **NEO@H1** and **PYR@H1**, respectively, indicating similar hydrodynamic radii before and after host–guest binding. Moreover, there are two representative conformers for the host–guest complexes for **NEO@H1** and **PYR@H1**, and the conformation of the host–guest complexes were determined based on NOE signals between the host and guest observed in the rotating Overhauser effect spectroscopy (ROESY) experiments (Fig. S4 and S5†).

Electrospray ionization mass spectrometry experiments were conducted to analyze the equimolar mixture of **H1** and the cationic guests **NEO**·BarF or **PYR**·BarF. The ESI mass spectrum revealed two intense peaks: one corresponding to $[\mathbf{NH_4@H1}]^+$ (m/z ~1458.7160) and the other to $[\mathbf{NEO}\subset\mathbf{H1}]^+$ (m/z 1663.8251, Fig. 3a) or $[\mathbf{PYR}\subset\mathbf{H1}]^+$ (m/z 1621.7771, Fig. 3b). These results confirm the formation of host–guest complexes through ESI mass analysis.

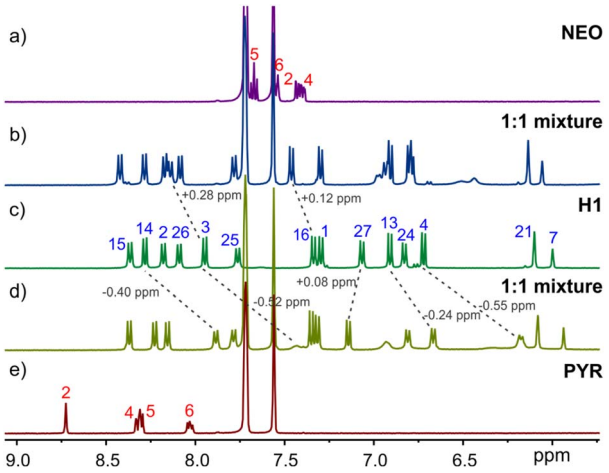

Fig. 2 Partial ^{1}H NMR spectra (500 MHz, CD_2Cl_2, 1.0 mM, 25 °C) of (a) NEO, (b) a 1 : 1 mixture of H1 and NEO, (c) H1, (d) a 1 : 1 mixture of H1 and PYR, and (e) PYR.

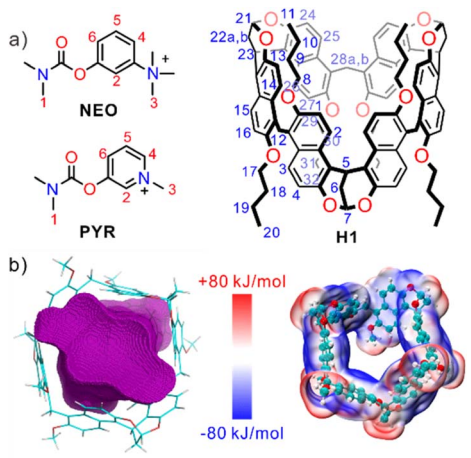

Fig. 1 (a) Structures of host H1 and guests (NEO, PYR); (b) the cavity volume (left) calculated by MoloVol and electrostatic potential surface (right) calculated by Multiwfn with ωB97XD/6-311G(d) method.

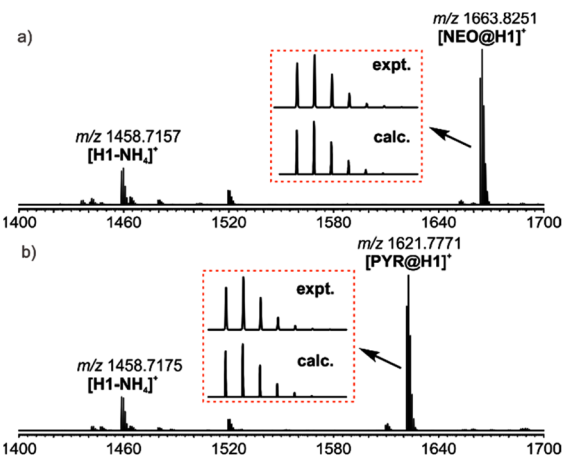

Fig. 3 ESI mass spectrum of 1 : 1 mixture of H1 and NEO (a) or PYR (b).

NMR titration experiments were then conducted to determine the association constants for the host–guest systems, as the formation of complexes occurs in a fast exchange on the NMR timescale. The titrations were performed using solutions with fixed and varying concentrations of the host molecule **H1** and the guest molecules (**NEO** and **PYR**), respectively. For example, when examining the guest **NEO**, it was observed that upon its addition, the chemical shifts of protons 3, 15, and 16 on the host exhibited significant changes, making them particularly amenable to monitoring (Fig. 4a). By fitting these variations in chemical shifts to corresponding guest concentrations based on a 1 : 1 binding model (Fig. 4b), we calculated three K_a values (2.83×10^4 M^{-1}, 2.69×10^4 M^{-1} and 2.68×10^4 M^{-1}), which are consistent with each other. We also analyzed the NMR titration data using the Musketeer software[15] developed by Hunter group, and the fitting result is similar with above results (Fig. S6†). Similarly, we determined the binding constant of **PYR** using the same method (Fig. S7†), which was found to be 2.2×10^5 M^{-1}. This value is an order of magnitude higher than that of **NEO** and aligns with the predictions obtained from the 1 : 1 NMR analysis. The strong binding affinity of methylene-bridged naphthotube towards these two drug molecules also establishes a foundation for its application as an ion carrier in electrochemical detection.[16]

ISEs are typically constructed from PVC-based membranes doped with plasticizers, ion exchangers, and ionophores.[17] Ion exchangers and ionophores improve selectivity;[18] the latter should possess a strong binding affinity for the target analyte, thus lowering the free energy required for its permeation through the aqueous membrane interface. This study prepared two membrane electrodes to assess the efficacy of methylene-bridged naphthotubes as ionophores for **NEO** and **PYR**. The fabrication method was based on established protocols, employing PVC, *ortho*-nitrophenyl octyl ether (*o*-NPOE) and potassium tetrakis[3,5-bis(trifluoromethyl)phenyl] borate as the polymer matrix, plasticizer, ion exchanger, respectively. **H1** functioned as the ionophore, while a control "blank" sensor contained no ionophores. Bu_4N^+ served as a reference compound due to its common use in potentiometry for evaluating ionophores owing to its high hydrophobicity. The more effective **NEO**/**PYR** ionophore was determined by comparing responses across different formulations (Fig. S8†). The potential differences were measured as electromotive force (EMF) values among **ISEs**: one without an ionophore and one containing **H1** for **NEO** and **PYR** relative to Bu_4N^+. The electrodes with **H1** displayed smaller potential differences than the blank electrode, indicating that its incorporation significantly reduces the free energy needed for **NEO** and **PYR** permeation across the aqueous membrane interface.

After confirming the efficacy of the ionophore, we proceeded to optimize the selection of plasticizer and working pH. The results indicated that *o*-NPOE demonstrated markedly superior sensitivity as a plasticizer in comparison to dioctyl sebacate (Fig. S9†). This finding underscores the importance of plasticizer choice in enhancing sensor performance. During the pH optimization process, We observed that within the pH range of 2 to 11, the potential responses of the two sensors are remarkably stable (Fig. S10†). Consequently, these types of sensors exhibit an extensive operational pH range.

In subsequent experimental procedures, a specific volume of a standard solution (0.1 M) containing the analyte was introduced into the buffer at intervals of 100 seconds while undergoing magnetic stirring. Potential responses were recorded within an analyte concentration range of 10^{-8}–10^{-2} M (Fig. 5a). The outcomes indicate that the potential response is swift and attains equilibrium almost immediately upon alterations in the analyte concentration. This rapid equilibration can be attributed to the fast equilibrium at the membrane/solution interface. Based on these potential responses, a calibration curve was established for the concentration range of 10^{-8}–10^{-2} M (Fig. 5b). Following the recommendations of the International Union of Pure and Applied Chemistry (IUPAC), the detection limit at 1 μM coincides with the intersection point of the linear response range, adhering to both the Nernst equation and regions of non-responsiveness. Compared to a blank electrode devoid of ion carriers, the electrode employing **H1** as an ionophore demonstrates a reduced detection limit and a steeper slope (Fig. S11†). This enhancement is primarily attributed to

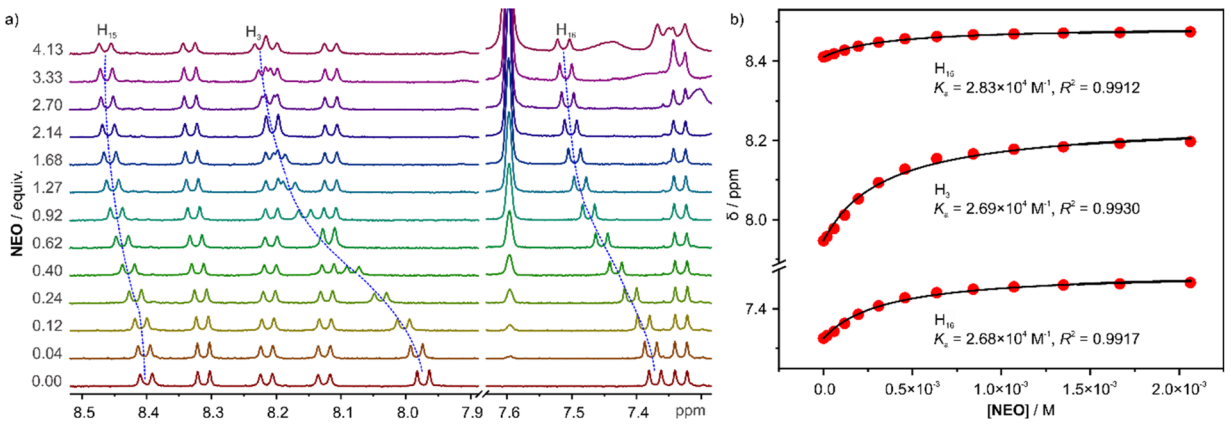

Fig. 4 (a) Partial ^{1}H NMR spectra (500 MHz, CD_2Cl_2, 298 K) of **H1** titrated with different concentrations of **NEO**. (b) The non-linear fitting of three proton signals against concentrations of **NEO** using a 1 : 1 binding model.

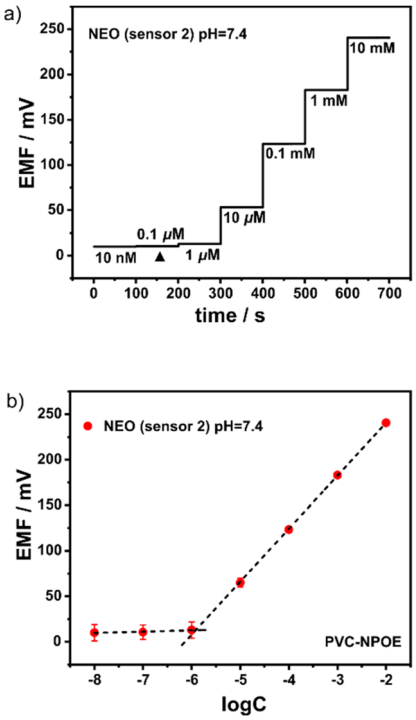

Fig. 5 (a) Response of EMF to incremental changes in the **NEO** concentration. (b) Calibration curves of the **H1**-based electrode to **NEO**.

the robust host–guest interaction between **H1** and the analyte's ester bonds. After completing the study on **NEO**, a response standard curve for **PYR** was constructed using a similar methodology. The measurements indicated a linear range of 10^{-6} to 10^{-2} mol L^{-1}, with a slope of 58.52 ± 0.52 mV per decade and a detection limit of 1.0×10^{-6} mol L^{-1} (Fig. S12†). Although the result is higher than the reported value,[9] this electrode system demonstrates rapid response characteristics and are adequate in detecting these two substances thereby facilitating the accurate determination of **NEO** and **PYR** in real-world samples.

To further investigate the performance of the membrane electrode sensor, systematic tests were conducted to evaluate its selectivity and anti-interference capabilities. The experiment selected common cations and representative amino acids as analytes, specifically Na^+, K^+, NH_4^+, Fe^{3+}, proline, histidine and glycine. As shown in Fig. 6, the electromotive force for **NEO** and **PYR** is significantly higher than that of other interfering substances. The calculated selectivity coefficients for various interfering substances (Table S1†) indicate that the selectivity coefficient values for the target substances are notably greater than those for other interferents. This suggests that the sensor exhibits high selectivity and good anti-interference capability towards the target substances. The primary reason for this selectivity is that the electron-rich deep cavity of **H1** can form specific host–guest complexes with the organic cations of **NEO** and **PYR** through weak interactions such as cation-π interactions. This mechanism implies that in a mixed system containing multiple substances, the membrane electrode preferentially interacts with **NEO** and **PYR**, thereby enhancing

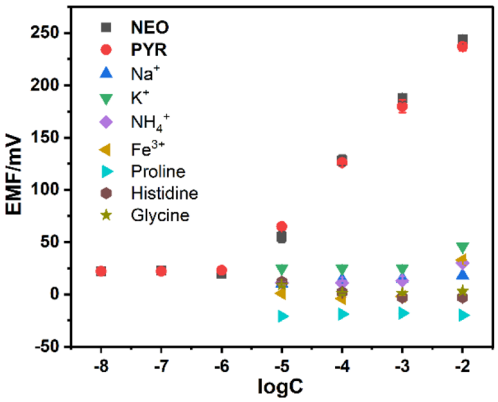

Fig. 6 The selectivity for **NEO** and **PYR** over Na^+, K^+, NH_4^+, Fe^{3+}, proline, histidine, and glycine of the electrodes containing **H1**.

detection selectivity. A comparative analysis with reported sensors[9] reveals that the present system demonstrates comparable or superior selectivity parameters, suggesting significant potential for real-sample detection applications.

To investigate the detection performance of our sensor in complex samples, we first attempted to detect **NEO** and **PYR** in fetal bovine serum. Three concentrations of **NEO** and **PYR** were prepared using the spiking recovery method. The experimental results indicated that the sensor responded quickly within the fetal bovine serum matrix, and the results were accurate and reliable, with recoveries ranging from 98% to 102% (Table 1). This demonstrates that the sensor is effective for detecting **NEO** and **PYR** in complex biological samples. Furthermore, in the field of pharmaceutical analysis, precise determination of drug component content is crucial for ensuring drug quality. We subsequently examined the application performance of the sensor in measuring drug content in methanesulfonate injection of neostigmine and bromide tablets. The results showed that the measured contents were consistent with the labeled amounts on the drug packaging, with recoveries generally exceeding 95% (Table S2†). This indicates that this analytical method has significant potential for application in pharmaceutical analysis.

In conclusion, to achieve rapid and efficient detection of **NEO** and **PYR**, we have successfully engineered an advanced ion-selective electrode membrane sensor utilizing methylene-bridged naphthotube as ionophore. This sensor exhibits exceptional sensitivity and selectivity, while eliminating the

Table 1 Determination of **NEO** and **PYR** in real samples

Samples	Added (μM)	Found[a] (μM)	Recovery (%)
PYR	10.0	10.0	100.0 ± 1.8
	100.0	98.0	98.0 ± 1.6
	1000.0	990.0	99.0 ± 1.1
NEO	10.0	10.2	102.0 ± 2.3
	100.0	98.0	98.0 ± 1.7
	1000.0	980.0	98.0 ± 1.5

[a] Mean value ($n = 3$).

need for sample preparation, thereby offering a robust technique for the rapid and accurate detection of **NEO** and **PYR**. With a minimum detection limit of 1.0 μM, it stands out as a promising analytical tool. Furthermore, its cost-effectiveness and environmentally friendly characteristics position it as a highly attractive option in the realm of pharmaceutical analysis, likely to gain significant traction in the field.

Data availability

The datasets supporting this article have been uploaded as part of the ESI.†

Conflicts of interest

There are no conflicts to declare.

Acknowledgements

This research was funded by National Natural Science Foundation of China (no. 22174059), Hunan Provincial Natural Science Foundation of China (no. 2022JJ40363), and the Young Science and Technology Innovation Program of Hunan Province (no. 2022RC1230). The APC was funded by University of South China.

Notes and references

1 (*a*) G. Pepeu and M. Giovannini, *Curr. Alzheimer Res.*, 2009, **6**, 86–96; (*b*) Q.-S. Yu, H. W. Holloway, W. Luo, D. K. Lahiri, A. Brossi and N. H. Greig, *Bioorg. Med. Chem.*, 2010, **18**, 4687–4693.

2 (*a*) A. S. Habib and T. J. Gan, *CNS Drugs*, 2006, **20**, 821–839; (*b*) N. Tajaate, J.-U. Schreiber, T. Fuchs-Buder, Y. Jelting and P. Kranke, *Eur. J. Anaesthesiol.*, 2018, **35**, 184–192.

3 M. Takahiro, O. Masaki, N. Toshiaki, I. Yuji and A. Takao, *J. Pharm. Biomed. Anal.*, 2006, **40**, 331–337.

4 K. Mariitta, *J. Chromatogr. A*, 1993, **648**, 501–506.

5 T. Sakai, X. Q. Liu and Y. Maeda, *Talanta*, 1999, **49**, 997–1001.

6 (*a*) E. P. Diamandis and T. K. Christopoulos, *Anal. Chim. Acta*, 1983, **152**, 281–284; (*b*) K. A. Fouad and Y. M. Issa, *Pharm. Biosci. J.*, 2015, **3**, 30–39.

7 F. Varin, J. Couture and H. Gao, *Biomed. Sci. Appl.*, 1999, **732**, 319–323.

8 (*a*) M. K. A. El-Rahman, H. E. Zaazaa, N. B. ElDin and A. A. Moustafa, *Talanta*, 2015, **132**, 52–58; (*b*) G. A. E. Sayed, M. R. Abukhadra, S. M. Mostafa, M. Rabia, M. A. Koranya and M. M. Khalil, *RSC Adv.*, 2023, **13**, 34715–34723; (*c*) A. A. Mouhamed, B. M. Eltanany, N. M. Mostafa, T. A. Elwaie and A. H. Nadim, *RSC Adv.*, 2023, **13**, 23138–23146.

9 (*a*) A. M. El-Kosasy, M. Nebsen, M. K. A. El-Rahman, M. Y. Salem and M. G. El-Bardicy, *Talanta*, 2011, **85**, 913–918; (*b*) A. F. Khorshid and Y. M. Issa, *Biosens. Bioelectron.*, 2014, **51**, 143–149.

10 M. A. El-Sayed, *Sens. Actuators B: Chem.*, 2014, **190**, 101–110.

11 (*a*) X.-N. Han, Y. Han and C.-F. Chen, *Chem. Soc. Rev.*, 2023, **52**, 3265–3298; (*b*) Z.-Y. Zhang and C. Li, *Acc. Chem. Res.*, 2022, **55**, 916–929; (*c*) Q. Shi, X. Wang, B. Liu, P. Qiao, J. Li and L. Wang, *Chem. Commun.*, 2021, **57**, 12379–12405; (*d*) S. Bleus and W. Dehaen, *Coord. Chem. Rev.*, 2024, **509**, 215762; (*e*) Y.-H. Tian, H. Qin, M.-H. Ding, L.-L. Tang and F. Zeng, *RSC Adv.*, 2023, **13**, 14539; (*f*) F. Zeng, L.-L. Tang, H. Yu, F.-P. Xu and L. Wang, *Chin. Chem. Lett.*, 2023, **34**, 108304; (*g*) C. Ruan, Z. Li, W. Lin, W. W. Xie, H. Li, Y. Lu, R. Wang, S. Li and L. Wang, *Org. Lett.*, 2024, **26**, 4122.

12 (*a*) P. D. Sala, R. D. Regno, C. Talotta, A. Capobianco, N. Hickey, S. Geremia, M. D. Rosa, A. Spinella, A. Soriente, P. Neri and C. Gaeta, *J. Am. Chem. Soc.*, 2020, **142**, 1752–1756; (*b*) L. P. Yang and W. Jiang, *Angew. Chem., Int. Ed.*, 2020, **59**, 15794–15796.

13 (*a*) Y. F. Wang, H. Yao, L. P. Yang, M. Quan and W. Jiang, *Angew. Chem., Int. Ed.*, 2022, **61**, e202211853; (*b*) Mi. Yan and J. Zhou, *Org. Chem. Front.*, 2023, **10**, 2340.

14 (*a*) L. P. Yang, X. Wang, H. Yao and W. Jiang, *Acc. Chem. Res.*, 2019, **53**, 198–208; (*b*) C.-D. Zhao, H. Yao, S.-Y. Li, F. Du, L.-L. Wang and L.-P. Yang, *Chin. Chem. Lett.*, 2024, **35**, 108879; (*c*) Y.-F. Wang, S.-M. Wang, X. Zhang, H. Nian, L.-S. Zheng, X. Wang, G. Schreckenbach, W. Jiang, L.-P. Yang and L.-L. Wang, *Angew. Chem., Int. Ed.*, 2023, **62**, e202310115; (*d*) S.-M. Wang, Y.-F. Wang, L. Huang, L.-S. Zheng, H. Nian, Y.-T. Zheng, H. Yao, W. Jiang, X. Wang and L.-P. Yang, *Nat. Commun.*, 2023, **14**, 5645.

15 D. O. Soloviev and C. A. Hunter, *Chem. Sci.*, 2024, **15**, 15299.

16 Y. Lu, S.-M. Wang, S.-S. He, Q. Huang, C.-D. Zhao, S. Yu, W. Jiang, H. Yao, L.-L. Wang and L.-P. Yang, *Chem. Sci.*, 2024, **15**, 14791.

17 (*a*) S. Ogawara, J. L. Carey, X. U. Zou and P. Bühlmann, *ACS Sens.*, 2015, **1**, 95–101; (*b*) Y. Ishige, S. Klink and W. Schuhmann, *Angew. Chem., Int. Ed.*, 2016, **55**, 4831–4835.

18 Q. Chen, L.-P. Yang, D.-H. Li, J. Zhai, W. Jiang and X. Xie, *Sens. Actuators B: Chem.*, 2021, **326**, 128836.